Investigation of Oxygen Reduction Reaction Kinetics at (111)−(100) Nanofaceted Platinum Surfaces in Acidic Media

Vladimir Komanicky, Andreas Menzel, and Hoydoo You*

Materials Science Division, Argonne National Laboratory, 9700 South Cass Avenue, Argonne, Illinois 60439

Received: July 27, 2005; In Final Form: October 10, 2005

The oxygen reduction reaction (ORR) was studied on CO-treated and untreated (111)−(100) nanofaceted platinum surfaces [Komanicky et al. *J. Phys. Chem.* **2005**, *109*, 23543] in sulfuric and perchloric acids using the rotating disk electrode technique. Activities of nanofaceted surfaces are found to be considerably higher than a simple average of the activities of (111) and (100) surfaces. We find that the high activity in sulfuric acid is consistent with the higher activity of (111) facets. It is due the weaker sulfate adsorption on finite-size (111) surfaces than on (111) single crystal surfaces where the ORR activity is suppressed by strong sulfate adsorption. However, the high activity found in the weakly absorbing perchloric acid cannot be explained by the finite-size effect, since the activities are reportedly insensitive to terrace sizes [Macia, M. D.; et al. *J.* Electroanal. Chem., **2004**, *564*, 141]. We propose a cooperative activity, unique to nanoscale objects, which results from oxy species crossing over between adjacent facets in nanometer proximities.

1. Introduction

The oxygen reduction reaction (ORR) is one of the most studied reactions in modern electrochemistry because it is important to a wide range of technological applications including energy conversion and corrosion prevention. The so-called particle size effect on the ORR kinetics has been long debated in electrocatalysis. A number of research groups tried to correlate nanoparticle size with the activity for oxygen reduction, often reporting contradictory results. Ross[1] and Peuckert et al.[2] reported the largest mass-specific activity at a particle size of ∼3 nm, which was rationalized by the largest faceted surface area per mass in a simple geometric analysis of cubooctahedra by Kinoshita.[3] On the other hand, Bett et al.[4] and Watanabe et al.[5] reported no correlation between particle sizes and activities. Watanabe et al.[5] offered an alternative explanation that when the nanoparticles are extremely small the diffusion fields of the nanoparticles may overlap and interfere each other, resulting in the low activity.

The lack of agreement between various authors is probably due to differences in experimental conditions and difficulties to precisely characterize these complex nanoparticle systems. Despite the controversy, however, the particle size effect in ORR is generally accepted especially after several recent studies[6−10] with Pt single crystal electrodes indicating that the structurally sensitive anion adsorption significantly changes the rates of ORR.

Although it is believed that anion adsorption is responsible for the particle size effect, there is no direct experimental evidence showing that the results obtained with large single crystals can be applied to nanoparticle surfaces. This argument is especially important since it is well-known that the anion adsorption is sensitive to the size of the platinum terrace.[10,11] Macia et al.[10] evaluated the dependence of the ORR kinetics on the size of the Pt terrace in the [01$\bar{1}$] zone. Unfortunately it is not possible to have nanosize terraces without a high step density, which introduces another factor possibly difficult to account for. In addition, stepped surfaces with only one crystallographic type of terraces cannot be used to study a possible crossover of the reacting species from one type of facet to another, which might be important in case of real catalysts composed of several varieties of the surfaces joined together.

In the preceding paper[12] we described a technique of preparing platinum single-crystal surfaces consisting of alternating rows of (111) and (100) nanofacets. In this paper we investigated ORR kinetics at the nanofaceted surface in a rotating disk electrode (RDE) configuration in sulfuric and perchloric acids. Influence of the surface defects on the kinetics of ORR in these electrolytes also will be discussed. We will show that the amount of the defects on the (111)−(100) nanofaceted Pt surfaces dramatically affects the rate of ORR in sulfuric acid. Contrarily, the defects do not have a pronounced effect on the rate of the oxygen reduction in perchloric acid.

2. Experimental Section

The nanofaceted surfaces for electrochemistry measurements were prepared according to the following procedure. Pt(1+$\sqrt{3}$ 1 1) single crystal was initially inductively annealed at ∼1900 K in argon/hydrogen flow for 15 min. This surface has always been used as a starting point for preparation of (111)−(100) nanofaceted surfaces described further in the text. The faceting of the surface was induced by annealing in ultrapure air at elevated temperatures. The (111)−(100) nanofaceted Pt surface with the wedge-to-wedge distance ∼12 nm was prepared by annealing the initial surface for 15 min at 1250 K. The crystal was then cooled to ∼600 K in the ultrapure air and then cooled to room temperature in research-grade argon (99.9995%) and brought in contact with supporting electrolyte at open circuit potential. All electrolyte solutions were prepared from J. T. Baker Ultrex II reagents and 18 MΩ cm^{-1} water purified by a Mili-Q reagent water system. Carbon monoxide (99.995%) was purged through the solutions for 10 min while electrochemical potential was held at 0 V. The electrode was then removed with a protective droplet of CO-saturated electrolyte from the

* Corresponding author. E-mail: hyou@anl.gov.

10.1021/jp054155a CCC: $30.25
Published on Web 11/17/2005

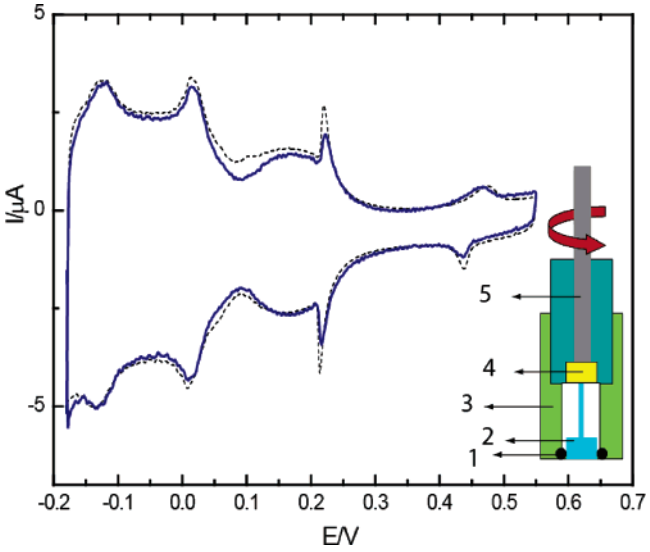

Figure 1. Cyclic voltammograms of a Pt (111) electrode sealed in the rotating disk assembly in 0.2 M sulfuric acid at 25 mV/s before rotation (dashed line) and the 5th CV during rotation (solid line) at 1600 rpm. Inset: Schematic diagram of the rotating disk assembly. 1. Kalrez O-ring, 2. Platinum crystal. 3. Teflon collet, 4. Press-on gold electrical contact between platinum crystal and rotator shaft, 5. Rotator shaft.

electrochemical cell[12] and immediately immersed in CO-saturated electrolyte in a Teflon container. Then, a Teflon collet was placed over the crystal which was subsequently inserted into the collet by pulling its pigtail. The collet with the crystal was then mounted on the RDE rotator (Pine Instrument Company). The complete assembly is shown as the inset of Figure 1. During this procedure the crystal was always protected by CO-saturated electrolyte. The RDE cell was filled with argon-purged electrolyte, and the electrolyte was replaced several times before a blank cyclic voltammogram (CV) was recorded without rotation. The blank CV was always recorded prior to the ORR kinetics measurements to verify the surface cleanness. The solution was then finally replaced with electrolyte saturated with oxygen at 1 atm and 25 °C. The contribution of the edge of the crystal to the current response was maintained as small as possible by sealing the crystal in the Kalrez O-ring. The geometrical surface area of the crystals was 0.159 cm^2 and all voltammograms were recorded at sweep rate of 25 mV/s. All potentials were referenced to the saturated Ag/AgCl reference electrode. The double junction and Luggin capillary was used to prevent the contamination of the cell by chlorides.

To verify that the surface cleanness is maintained during rotation, we compare the blank CV of Pt(111) electrode in 0.2 M sulfuric acid before rotation and the CV during rotation at 1600 rpm in Figure 1. The CV before rotation (shown by the dashed line) indicates that the surface of the electrode remained clean during the transferring and mounting procedure. The fifth CV obtained during rotating at 1600 rpm is shown by the solid line for comparison. Presence of the current spike at 0.22 V in this cyclic voltammogram proves that the solution purity is very high and that we could maintain a clean surface during RDE measurement. We used Kalrez O-ring seal to minimize the current from the side of the crystal. The slight unavoidable contribution of the edge can be seen as two small peaks in the hydrogen absorption region of the CV.

The surface morphology was always checked with AFM *after* each ORR measurement to confirm the expected morphology of the nanofaceted surface. Two AFM images obtained in two separate measurements are shown in Figure 2 to demonstrate the reproducibility. We were able to consistently obtain the reproducible surface morphology by precisely controlling the annealing temperature and time.

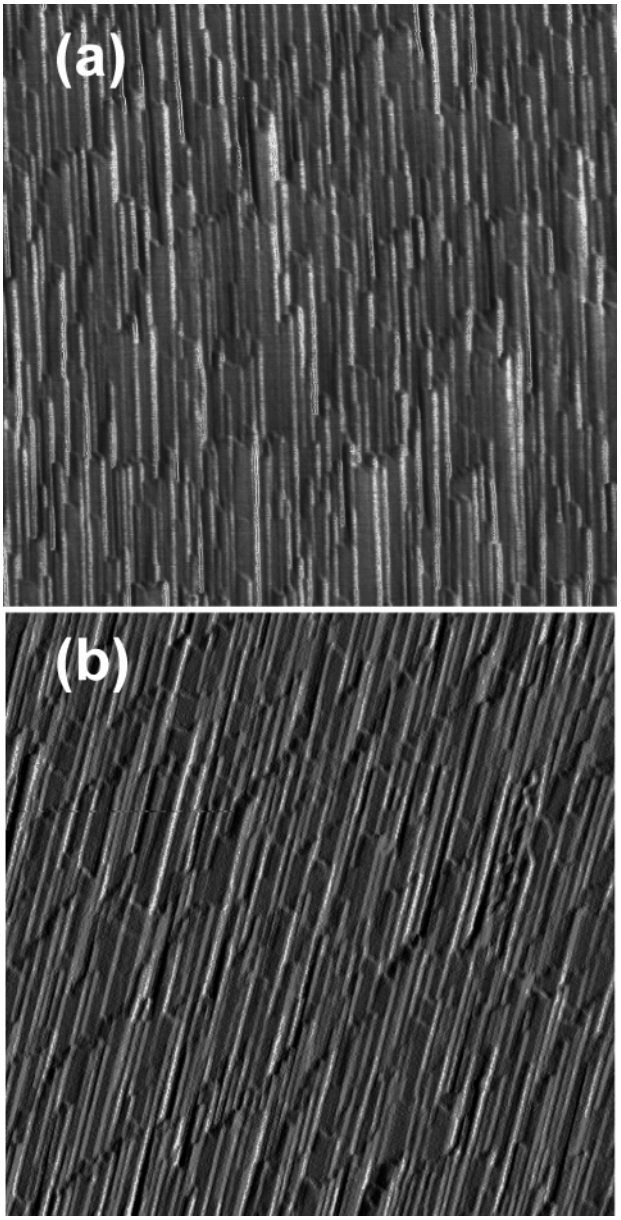

Figure 2. AFM images (1×1 um^2 area shown) of two (111)−(100) nanofaceted surfaces demonstrating the reproducibility of our annealing procedure. Both surfaces were flat and featureless by annealing initial hydrogen/argon annealed Pt($1+\sqrt{3}$ 1 1) surface. The images were obtained after annealing in ultrapure air at 1250 K for 15 min.

3. Results

3.1. Rotating Disk Electrode Technique for Study of Oxygen Reduction Reaction. Since the solubility of oxygen (2.293×10^{-5} mol fraction)[13] at room temperature in aqueous electrolytes is quite low ORR kinetics is easily limited by diffusion in a stationary hanging-meniscus geometry. For this reason, the previous studies of ORR kinetics were typically performed using RDE geometries where one can vary the saturation level of the oxygen supply to the surface by varying rotating speed.[6]

The kinetic current density, i_k, the diffusion-limited current density, i_d, and the measured current density, i, at RDE for a first-order reaction under mixed kinetics/diffusion control have

the following relationship:

$$\frac{1}{i} = \frac{1}{i_d} + \frac{1}{i_k} \quad (1)$$

where the diffusion-limited current density $i_d = 0.62nFD^{2/3}\nu^{-1/6}c_{bulk}\omega^{1/2}$; n is a number of exchanged electrons, F is a Faraday constant, D is the reactant diffusion coefficient, ν is the solution viscosity, c_{bulk} is the reactant concentration in the solution, and ω is the angular velocity of the RDE. The inverse kinetic current density, $1/i_k$, can be obtained from eq 1 as the intercept of Koutecký−Levich plots, $1/i$ vs $1/\omega^{-1/2}$, for a given potential.

Methods of transferring and mounting of single crystal electrodes into a rotating disk assembly have well been established.[6,7] In our measurements, therefore, we followed closely the established procedure and before we begin working with the nanofaceted surfaces we verified that our current−voltage curves of Pt(111) and (100) surfaces measured in perchloric and sulfuric acids all reproduce the previously reported ones.[6,7] Then the same procedures were repeated for the nanofaceted surfaces.

3.2. Selection of the Nanofaceted Surfaces and the Electrolytes. We chose the (111)−(100) nanofaceted surface prepared at 1250 K discussed in the preceding article[12] for our ORR measurements. This is chosen for the nanofacets' wedge-to-wedge distance of ∼12 nm, narrow enough so that the finite-size effects should be expected to present yet wide enough so that the nanofacets are clearly resolvable and reproducible with AFM measurements without having to use synchrotron X-rays to characterize. Typical AFM images are shown in the preceding article[12] and also are reproduced in Figure 2.

In the preceding article we have shown that the repeated CO adsorption−desorption cycles have effects similar to thermal annealing and remove efficiently defects from the surfaces. Since surface defects have long been considered to affect certain electrocatalytic activities, we performed two sets of experiments to examine the influence of surface defects on the ORR activities of the nanofaceted Pt surface: (1) the surface nearly defect-free, prepared as described in section 2 was treated by the CO adsorption−desorption cycles described in the preceding article; (2) the surface with significant amount of defects present annealed and cooled in the same manner but transferred to the RDE setup simply protected in CO-free electrolyte.

The range of ordering and the amount of adsorbed sulfate depends on the size of the Pt(111) domains.[10,12] Since a considerable amount of sulfate can adsorb on Pt(111) terraces only ∼5 atoms wide, e.g., Pt(322), anion effects are expected to influence the ORR kinetics. The integrated charge under current−voltage peaks at potentials above 0.17 V confirms that large amounts of sulfate can adsorb on the (111) nanofacets: 53 μC/cm^{-2} for electrochemically annealed (111)−(100) nanofaceted Pt surface vs 85 μC/cm^{-2} for Pt(111). We also performed experiments in perchloric acid, known to be more weakly adsorbing than sulfate, to evaluate the influence of the anion adsorption on the ORR kinetics at the (111)−(100) nanofaceted Pt surface.

In case of the electrode consisting of two different active surfaces, we consider the following two scenarios for the current−voltage response of the electrode. First, the ORR activities of both (100) and (111) nanofacets are so close that the whole surface area of the electrode is electroactive and the system behaves according to the Levich equation with linear dependence of $1/i$ vs. $1/\omega^{-1/2}$ at all potentials. This is the case for our data in sulfuric acid. Second, the difference between

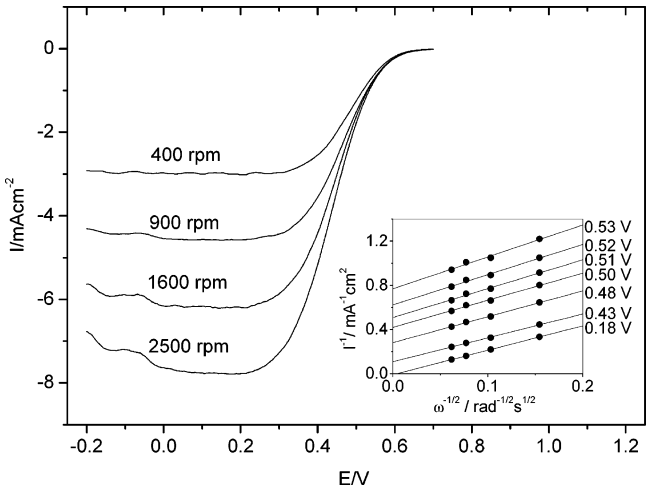

Figure 3. Current−voltage curves measured at 25 mV/s with a rotating disk electrode of the CO-treated (111)−(100) nanofaceted Pt surface for oxygen reduction reactions in 0.2 M sulfuric acid. Inset: Koutecký−Levich plot at different potentials in the kinetic-diffusion region of the polarization curve. The bottom line marks the diffusion-limited current region.

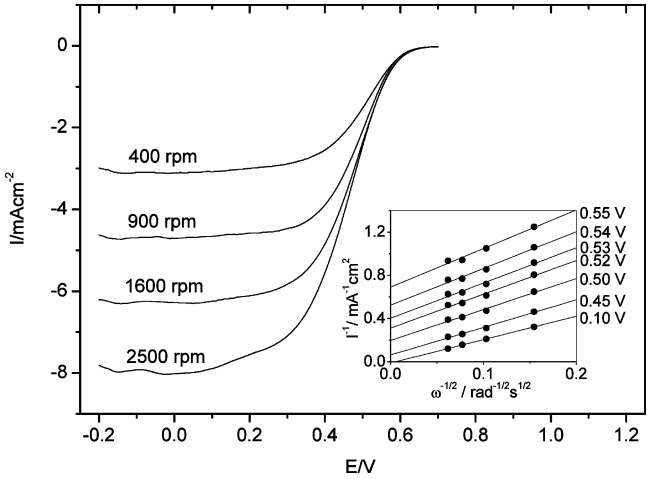

Figure 4. Current−voltage curves measured at 25 mV/s with a rotating disk electrode of the untreated (111)−(100) nanofaceted surface for oxygen reduction reactions in 0.2 M sulfuric acid. Inset: Koutecký−Levich plot at different potentials in the kinetic-diffusion region of the polarization curve. The bottom line marks the diffusion-limited current region.

activities of the (111) and (100) nanofacets causes deviations from the Levich equation. Current densities deviate from the Levich equation mostly at the beginning of the mixed kinetics/diffusion region of the polarization curve, where the ORR proceeds mainly on one type of the surface. This is the case of our data in perchloric acid.

3.3. Oxygen Reduction Reaction in Sulfuric Acid. The current−voltage curves measured at several different rotation speeds in oxygen-saturated sulfuric acid for the (111)−(100) nanofaceted Pt electrode with and without CO treatment are shown in Figure 3 and Figure 4, respectively. Reasonably linear Koutecký-Levich plots are obtained (see the insets) at all measured potentials where ORR is expected to be under the mixed kinetics/diffusion control, and the linear plot under the pure diffusion control (0.18 V) intercepts zero. This indicates that the electrochemical activities of both (111) and (100) nanofacets are very close. This is contrary to single-crystal results where a large difference in activities between (111) and (100) surfaces was found. However, it is consistent with the

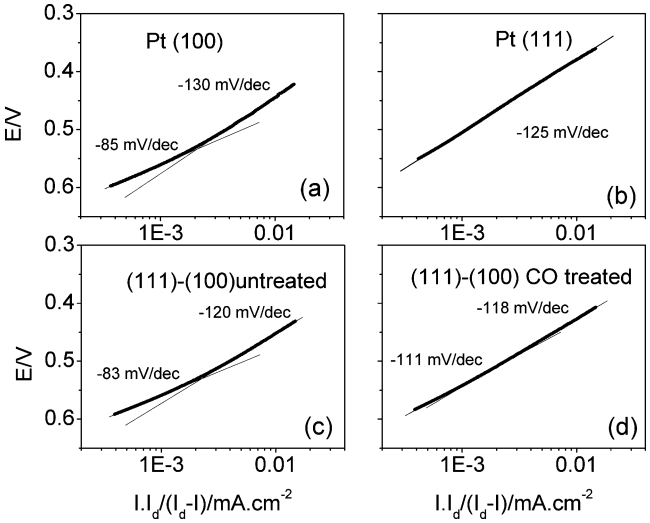

Figure 5. Tafel plots for the ORR at the CO-treated and untreated (111)−(100) nanofaceted surface and Pt(111) and Pt(100) in 0.2 M sulfuric acid. The kinetic currents were obtained from the current−voltage curves recorded at 900 rpm with the scan rate of 25 mV/s using eq 1.

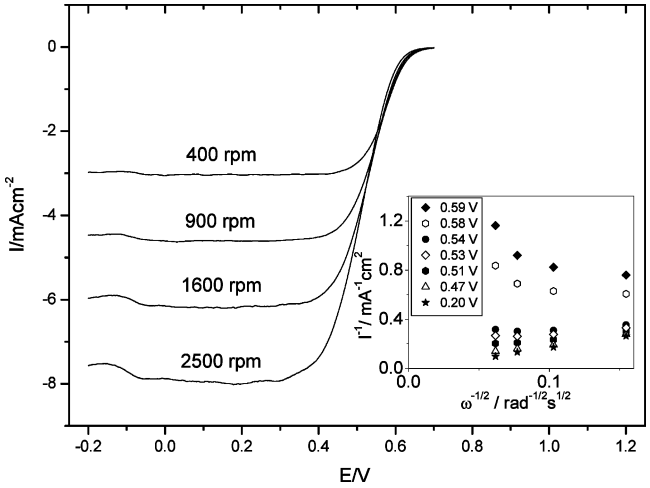

Figure 6. Current−voltage curves measured at 25 mV/s with a rotating disk electrode of the CO-treated (111)−(100) nanofaceted Pt surface for oxygen reduction reactions in 0.1 M perchloric acid. Inset: Koutecký−Levich plot at different potentials in kinetic-diffusion region of the polarization curve. The bottom data set marks the diffusion-limited current region.

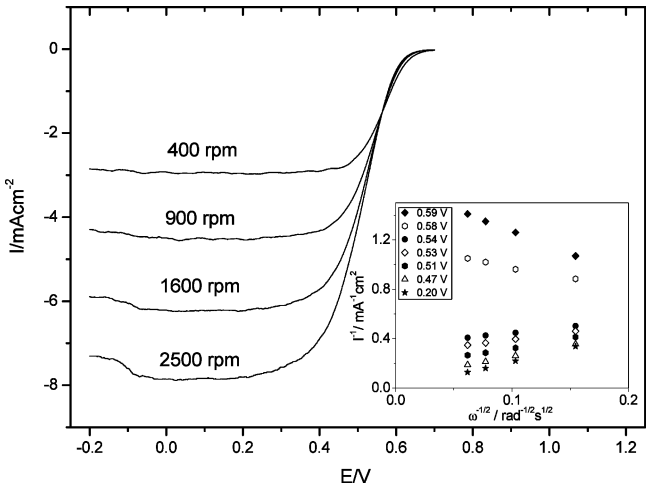

Figure 7. Current−voltage curves measured at 25 mV/s with a rotating disk electrode of the untreated (111)−(100) nanofaceted Pt surface for oxygen reduction reactions in 0.1 M perchloric acid. Inset: Koutecký−Levich plot at different potentials in kinetic-diffusion region of the polarization curve. The bottom data set marks the diffusion-limited current region.

results on stepped platinum (111) and (100) vicinal surfaces.[10] The activity initially suppressed by sulfate adsorption is increased when the terrace sizes become small, and the activity difference between stepped (100) and stepped (111) surfaces is at most ∼20 mV.

The kinetic currents for the (111)−(100) nanofaceted electrodes can be obtained from eq 1 in sulfuric acid because the activities of the two nanofacets are relatively similar. Therefore, we were able to construct Tafel plots in the case of sulfuric acid as shown in Figure 5. A break in the Tafel slope was observed in case of Pt(100) (Figure 5a), but a single Tafel slope of 125 mV per decade is found for Pt(111) in sulfuric acid (Figure 5b), which is very close to the theoretically calculated value of 118 mV per decade for a single electron transfer reaction. This indicates that the rate determining step is the transfer of one electron, which is most likely transfer of the first electron, to oxygen molecule:

$$O_{2(ads)} + e^- \xrightarrow{k2} O_{2(ads)}^- \qquad (2)$$

In contrast, the Tafel plots of (111)−(100) nanofaceted Pt electrodes show a change in the slope. As suggested previously,[6,8] this is not related to the change of the reaction mechanism but caused by the reversibly adsorbed $OH_{(ads)}$ in the case of the (100) surface. Higher density of steps and step-like defect sites will also result in higher $OH_{(ads)}$ coverages because OH adsorption is probably stronger at steps and defects on Pt(111) surfaces.[7,9] The break in the Tafel slope shown in Figure 5c for the untreated (111)−(100) nanofaceted surface decreases after CO treatments, as we can see in Figure 5d. This result indicates that a smaller number of $OH_{(ads)}$ species are present at the surface due to fewer defects.

3.4. Oxygen Reduction Reaction in Perchloric Acid. In oxygen-saturated perchloric acid, the current−voltage curves show an inversion at the foot of the polarization curves, i.e., the kinetic current *decreases* when rotation speed *increases*. The decrease is always reproduced, whether the current−voltage curves are recorded with stepwise increasing or decreasing rotation speed, and both in cathodic and anodic sweeps, albeit only cathodic sweeps are shown in Figure 6 and Figure 7. We think that it is caused by a large difference between the activities of (111) and (100) nanofacets. We made Tafel plots as we have done for the case of sulfuric acid, and they are shown in Figure 8. Tafel plots show large breaks even when the sample was CO-treated. Furthermore, Tafel plots for (111)−(100) nanofaceted Pt electrodes are shifted in the cathodic direction when the rotation speed is increased. As a result, nonlinear Koutecký−Levich plots (see the insets in Figure 6 and Figure 7) are obtained. One may argue that contamination of the solution could shift polarization curves at higher rotation speeds in the cathodic direction. If this was the case we should have observed the same trend with all electrodes, including Pt(111) and Pt-(100) electrodes. We did not see any shift with these electrodes and thus eliminate the possibility of contamination. In addition, we verified that the current decrease with the rotation speed increase was reproduced in both increasing and decreasing steps of rotation speed. This verification eliminates any possible poisoning of the surface by contaminants, which can cause the current inversion seen at higher rotation speed. Several consecutive current−voltage sweeps at the same rotation speed obtained

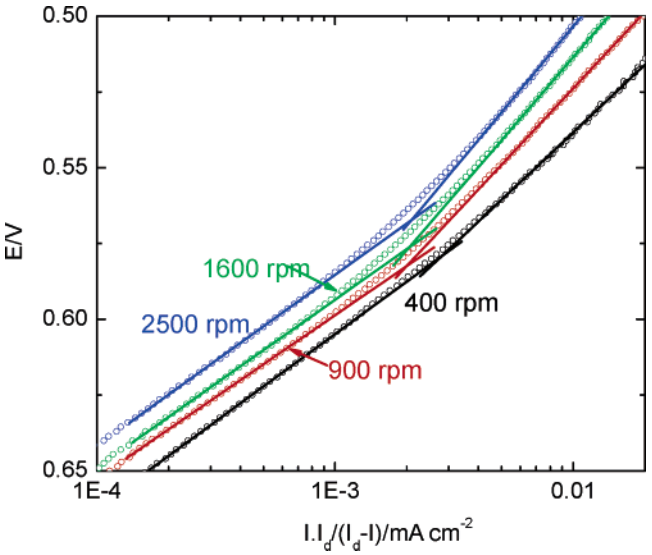

Figure 8. Tafel plots for CO treated (111)−(100) nanofaceted Pt electrode obtained at 400, 900, 1600, and 2500 rpm in 0.1 M $HClO_4$. Break in Tafel slope increases with increasing rotation speed. Following values of Tafel slopes were obtained. High current densities and increasing rotation speed: 74 mV/dec; 84 mV/dec; 90 mV/dec; and 95 mV/dec. Low current densities and increasing rotation speed: 57 mV/dec; 54 mV/dec; 56 mV/dec; and 56 mV/dec.

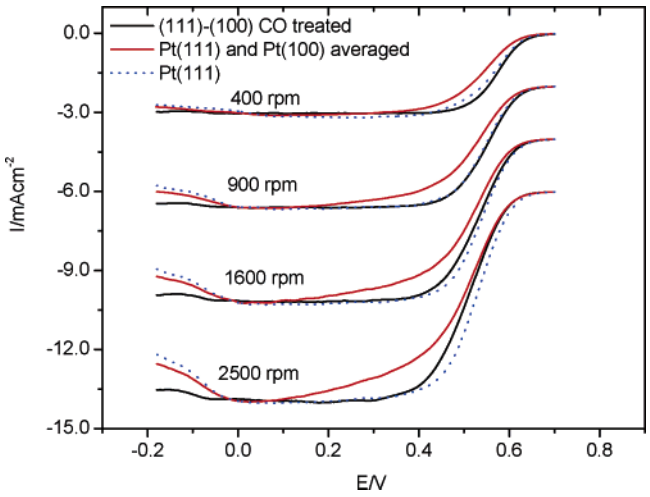

Figure 9. Current−voltage curves measured at 25 mV/s for the oxygen reduction reactions on the CO-treated (111)−(100) Pt electrode, those on Pt(111), and the averages of the curves for Pt(111) and Pt(100), in perchloric acid. The current−voltage curves at rotation speeds higher than 400 rpm were shifted vertically for better clarity.

for (111)−(100) nanofaceted Pt surface were identical (a fifth scan is shown in Figure 1), which additionally confirms the cleanness of the surfaces during rotation and also rules out the possibility of the roughening of the surface by formation of a platinum oxide layer at more positive potentials.

The difference between the oxygen reduction half wave potentials for stepped (111) and (100) surfaces in perchloric acid remains ∼100 mV,[10] even when the terrace sizes are similar to those of our (100)−(111) nanofacets, indicating that the terrace size plays only a minor role determining ORR activities. We believe, as we mentioned earlier, that the large difference in activities between the facets is responsible for the deviations from linear Koutecký−Levich behavior and the current inversion. The difference in the activities between (111) surfaces and (100) surfaces in perchloric acid has been suggested as a result of the lower affinity of $OH_{(ads)}$ to (111) surfaces than to (100) surface.[9,15,16] Therefore, we can consider our electrode inhomogeneous or partially active, at least within the potential range of ∼100 mV. In the next section, we will consider theoretical models of partially active surfaces and compare the theoretical results to our data.

4. Discussion

4.1. Rotating Disk Electrodes with Nonuniform Activities. The validity of the Levich equation for the case of a disk with partially active surface areas has been tested in simple geometries, such as circular active sites distributed on an inactive RDE by Landsberg and Thiele[18] and, more recently, an inactive film with circular pores covering an active RDE by Ahlberg et al.[19] According to their results, if the thickness of the diffusion layer δ_d is much larger than the length scales of electrode inhomogeneities, like in our case, reaction rates can simply be replaced by effective rates and currents still follow Koutecký−Levich type behavior, albeit one exception of the nonzero intercept even in the diffusion controlled potential region. However, our data shown in the insets of Figure 6 and Figure 7 exhibit significant deviations from the expected linear behavior. In addition, the current inversion seen in our data cannot be explained by such effective reaction rates or nonzero intercepts.

Rosner[20] considered another simple case of a disk with the inactive center where the active area is in the shape of a planar ring. In this case, the current density is always larger than the current density expected for a disk electrode of the same area. The increased current density results from an additional mass transport from the inactive center spilling over to the active ring area. Although the geometry considered by Rosner[20] is macroscopic and cannot be applicable to our case, the spillover of the reactant from the inactive part of the disk to the active part is analogous to our case where the crossover of the reactant from the inactive (100) facets to the active (111) surface is expected. His analysis indicates indeed the larger fractional increase, not absolute increase, of the diffusion current at a low rotation speed than at a high rotation speed. However, it still cannot explain the current inversion seen in our data requiring the absolute increase in current densities at lower rotation speed.

In both cases of partially active surfaces, the reactants from the inactive part of the surface are allowed to move to the active part either by diffusion[18,19] or by convection.[20] However, possible interactions or inter-diffusion of the reactants and intermediates between the active and inactive parts of the electrode surface have not been considered. To explain our data, we therefore discuss a possible scenario of cooperative reactions due to the inter-diffusion in the following section.

4.2. Cooperative Reactions between (111) and (100) Nanofacets in Perchloric Acid. We suggest the possibility of cooperative reactions between two facets with different activities in close proximity, which is unique to nanoscale objects such as real catalysts. If there is significant exchange of reactants and intermediates between the nanofacets, the cooperative interactions can lead to an overall higher activity for the nanofaceted surface than for either facet species alone. The activity can be enhanced by feeding reactants and intermediates from the less active surface to the more active surface at a given reaction step.

The high activities of the nanofaceted surface can be seen in the RDE measurements. Figure 9 shows current−voltage curves for the CO-treated (111)−(100) nanofaceted Pt electrode overlaid with the current−voltage curves for Pt(111), which is

more active than the (100) surface, and with the average of the current−voltage curves of (111) and (100) single crystal electrodes. We used the rates for the single crystal surfaces because the ORR rates on the narrow (111) and (100) terraces are essentially identical to those on corresponding single-crystal surfaces.[10] Note that the measured currents of the (111)−(100) nanofaceted Pt electrode are larger in all rotation speeds than the averages and very close to the currents of Pt(111) electrode. At the highest rotation speed in the mixed kinetics/diffusion potential region (at the foot), the current−voltage curve for the nanofaceted surface, and the average overlay quite well. This suggests that, at low rotation speeds, the whole surface behaves like Pt(111) or better, but at high rotation speeds it behaves like the sum of two independent facets. We believe this is because the crossover rates are no longer significant compared to the reaction rates at high rotation speeds. We suggest that the break in the Tafel slope becomes larger with increasing rotation speed (see Figure 8) due to the larger contributions from the (100) surface. The linear fits with two lines with different slops were made to each Tafel plot. The fits are qualitative, but there are systematic increases of (i) the Tafel slope and (ii) the slop change at the breakage where rotation speed at high current density is easily recognizable. Normally, Tafel plots at different rotation speeds are expected to overlay almost precisely, as was the case of all investigated electrodes in sulfuric acid.

Let us apply the general behavior discussed above to the more specific steps of ORR in order to illustrate the possible consequences of the crossovers. Furthermore, we adopt the sequence of reaction steps shown below[21] for our discussion. However, we emphasize that our main conclusion, the cooperative reactions by the crossover, does not depend on the validity of the following sequence or the validity of our choice of these steps for this illustration. The remaining steps and numerous possible alternative reaction pathways are not shown here for simplicity.

$$O_2 \xrightarrow{k1} O_{2(ads)} \quad \text{(i)}$$

$$O_{2(ads)} + e^- \xrightarrow{k2} O^-_{2(ads)} \quad \text{(ii)}$$

$$O^-_{2(ads)} + H_2O \xrightarrow{k3} HO^-_{2(ads)} + OH_{(ads)} \quad \text{(iii)}$$

When the potential is changed in cathodic direction, the ORR first starts at (111) nanofacets since the (111) surface is more active in perchloric acid than the (100) surface. Now we hypothesize that, at low oxygen supply, step (i) is rate limiting for the (111) facets, while for the (100) facets step (ii) is rate limiting. In this case, the excess oxygen molecules of the (100) facets can crossover to the (111) surface and be consumed. Therefore, the whole nanofaceted surface is as active as the (111) facets. Furthermore, if the affinity of molecular oxygen to the (100) facets is larger[16] than that of the (111) facets, the overall reaction can even be larger than the reaction rate of the (111) facets. In this hypothetical situation, we can rationalize the 400-rpm data.

As the oxygen flux increases at higher rotation speeds, the production of the $OH_{(ads)}$ species increases at the (111) nanofacets. Then the $OH_{(ads)}$ species generated in step (iii) can cross over from (111) to (100) nanofacets and compete with the adsorption of molecular oxygen. This is more likely if the affinity of the $OH_{(ads)}$ species to the (100) facets is larger[16,17] than to the (111) facets. Since the binding energy of the $OH_{(ads)}$ is expected to be higher than that of the neutral molecular oxygen, the $OH_{(ads)}$ species effectively block the adsorption of molecular oxygen to the (100) facets, and the effect of crossover enhancement drops rapidly. The (100) facets free up the active sites and become active only when the potential is stepped to more negative values, and the reaction is limited by step (ii) as usual. Then the overall surface behaves more like the average surface combined of (111) and (100) facets since the reactions in each facet are essentially limited by their own rate-determining reaction steps. This cooperative mechanism is schematically illustrated in the Figure 10.

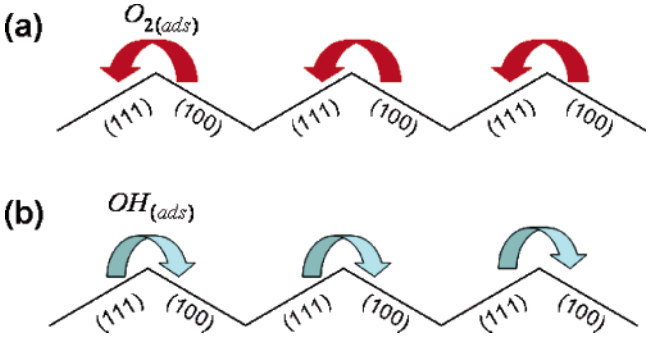

Figure 10. Schematic illustration of the cooperative mechanism of ORR on (111)−(100) nanofaceted Pt surface. (a) At low oxygen flux, excess oxygen or superoxide ion crosses over from (100) nanofacets to the supply-limited (111) nanofacets. (b) At high oxygen flux, (100) surface is being blocked by reaction intermediates such as OH_{ads} crossed over from (111) nanofacets to (100) nanofacets.

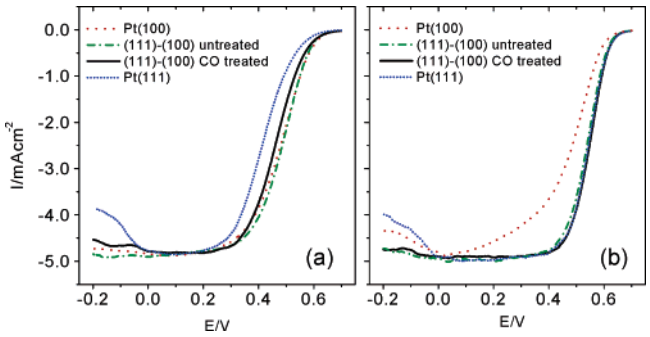

Figure 11. Current−voltage curves for ORR for the CO-treated and untreated (111)−(100) nanofaceted Pt surfaces, Pt(111) surface, and Pt(100) surface at 900 rpm, 25 mV/s in (a) 0.2 M sulfuric acid; (b) 0.1 M perchloric acid.

More complex scenarios for the crossovers of reactants, intermediates, and poisons can be considered. However, the above hypothetical example illustrates possible cooperative reactions that offer a possible explanation for the current inversion seen in our data. We believe that the current inversion might be explained only by the cooperative reactions discussed in this section and important to understanding the high activities of the nanoparticle platinum or platinum alloy electrocatalysts.

4.3. Effect of CO−Induced Annealing on Reaction Kinetics. The current−voltage curves for the CO-treated and the untreated (111)−(100) nanofaceted Pt surfaces in sulfuric acid and perchloric acid electrolytes at 900 rpm are directly compared in Figures 11a and b, respectively. The data for the Pt(111) and Pt(100) electrodes are also shown for comparison. The anodic shift of ~70 mV in the half-wave potential measured in perchloric acid compared to that in sulfuric acid for the CO-treated (111)−(100) nanofaceted Pt surface confirms the influence of anion adsorption on ORR kinetics. Since in perchloric acid both the CO-treated and untreated (111)−(100) nanofaceted Pt surfaces show similar activities, the amount of defects on the nanofacets does not have a strong effect on the rate of ORR.

TABLE 1: Kinetic Parameters Obtained at 900 rpm for the Oxygen Reduction at the CO-Treated and Untreated (111)−(100) Pt Nanofaceted Surfaces, Pt(111), and Pt(100)

	0.2 M H_2SO_4		0.1 M $HClO_4$	
h,k,l	$k \times 10^2$ (cm s^{-1})	$\Delta E/\Delta \log i$ (mV/dec)	$k \times 10^2$ (cm s^{-1})	$\Delta E/\Delta \log i$ (mV/dec)
Pt(111)	0.3	−125	5.1	−76
Pt(100)	1.3	$-130_{hcd}/-85_{lcd}$	1.4	$-121_{hcd}/-79_{lcd}$
Pt(111)−(100) CO treated	1.0	$-117_{hcd}/-102_{lcd}$	5.0	$-84_{hcd}/-54_{lcd}$
Pt(111)−(100)	2.3	$-120_{hcd}/-83_{lcd}$	3.5	$-98_{hcd}/-59_{lcd}$

On the other hand, in sulfuric acid the defects on the facets have a significant effect on the rate of ORR. The longer-range order on Pt(111) facets is reflected in slower ORR kinetics, which can be seen by a difference of ~20 mV between the half-wave potentials of the CO treated and untreated (111)−(100) nanofaceted surfaces.

The rate constants for ORR at the nanofaceted surfaces (see Table 1) were obtained from Koutecký−Levich plots at 0.47 V, where ORR is under mixed kinetics/diffusion control. The rate constants for large Pt(111) and Pt(100) surfaces are determined in the same way and are included for comparison. Taking into account the larger difference between the activities of (111) and (100) nanofacets in perchloric acid, this potential was chosen so that the slopes of the lines in the Koutecký−Levich plots are close to the ones at the diffusion-limited currents. In this case, one can average the intercepts obtained from the Koutecký−Levich plots to determine the "average" rate constant. The rate constants obtained in perchloric acid at 0.47 V for the CO-treated and untreated (111)−(100) nanofaceted Pt surfaces are very similar. Slightly lower activity of the untreated (111)−(100) nanofaceted surface might be attributed to the more negative onset potential of OH adsorption on rough surfaces. The trend is opposite in sulfuric acid where the activity of the (111)−(100) nanofaceted Pt electrode with a larger amount of the defects is increased by ~20 mV.

5. Summary

We have studied oxygen reduction reactions (ORR) on nanofaceted platinum surfaces with the RDE technique in perchloric and sulfuric acids. The surface was initially cut close to (311) and annealed at 1250 K in the presence of oxygen.[12] The surface splits into an array of alternating (100) and (111) narrow facets that are ~6 nm across and nearly 1 μm long. The experiments were performed with the CO-treated and untreated nanofaceted surfaces to examine the influences of surface defects on the nanofacets. The more sluggish rates of oxygen reduction on the CO-treated surface in sulfuric acid was attributed to the stronger anion adsorption effects due to the improved long-range ordering of the nanofacets. More than two-fold increase in the ORR rate at the nanofaceted Pt surface with higher amount of the defects can be related to the sensitivity of sulfate adsorption on the surface long range order. Contrarily, we find that the influence of the surface defects were much less significant in perchloric acid. Furthermore, the untreated surface with the higher amount of the defects was found to be slightly less active, not more active. We attribute this opposite behavior to the higher coverage of the facets by the $OH_{(ads)}$ species that are generally believed to hinder ORR.

In comparing only the CO-treated nanofaceted surfaces, we found that the ORR activity in sulfuric acid is higher than that of the (111) surface but less than that of the more active Pt-(100) surface. This indicates that the activity of the (111) facets is significantly enhanced. We attribute the enhanced activity of (111) facet to the finite-size effect[10,12] where the sulfate adsorption appears suppressed when the size of the terrace becomes a nanoscale. The overall ORR activity could be characterized with a single effective rate constant, as shown with a near straight line in the Koutecký−Levich plots. In perchloric acid, we observed a substantial overall increase of ORR activities, especially at low rotation speeds, leading to an inversion in the ORR rate at the foot of the current−voltage curves. The kinetic current actually decreases as the rotation speed is increased. We obtained nonlinear Koutecký−Levich plots that we propose are the result of the large difference between the activities of (111) and (100) nanofacets. Simple models with nonuniform surface activities[18−21] are found not to properly describe the nonlinearity in the Tafel plots and the inversion of the current−voltage curves seen in our studies. To reconcile the nonlinear Tafel plots and the current inversion, we propose a simple cooperative reaction scheme allowing crossover of reactants and intermediates between (111) and (100) facets. We believe the cooperative crossover reaction phenomena are possible due to the proximity of the nanofacets, are unique to the nanosize catalysts, and may occur in the real nanoparticle catalysts operating in electrochemical conditions or in gaseous reaction conditions.

Acknowledgment. This work was supported by the Materials Sciences Division of the Office of Basic Energy Science, and the use of Advanced Photon Source was supported by the Office of Basic Energy Sciences, U.S. Department of Energy under Contract No. W-31-109-ENG-38.

References and Notes

(1) Ross, P. N. In *Structure−Property Relations in Noble Metal Electrocatalysis*, LL-21733, LBL, 1986, Berkeley, CA.

(2) Peuckert, M.; Yoneda, T.; Dalla Betta, R. A.; Boudart, M. *J. Electrochem. Soc.* **1986**, *133*, 944.

(3) Kinoshita, K. *J. Electrochem. Soc*. **1990**, *137*, 845.

(4) Bett, J.; Lundquist, J.; Washington, E.; Stonehart, P. *Electrochim. Acta* **1973**, *18*, 343.

(5) Watanabe, M.; Saegusa, S.; Stonehart, P. *Chem. Lett.* **1988**, 1487.

(6) Markovic, N. M.; Gasteiger, H. A.; Ross, P. N. *J. Phys. Chem.* **1995**, *99*, 3411.

(7) Markovic, N. M.; Gasteiger, H. A.; Grgur, B. N.; Ross, P. N. *J. Electroanal. Chem.* **1999**, *467*, 157.

(8) Markovic, N. M.; Gasteiger, H. A.; Ross, P. N. *J. Phys. Chem.* **1996**, *100*, 6715.

(9) Markovic, N. M.; Ross, P. N. In *Interfacial Electrochemistry*; Wieckowski, A., Ed.; Marcel Dekker: New York, 1999; pp 827−828.

(10) Macia, M. D.; Campiña, J. M.; Herrero, E.; Feliu, J. M. *J. Electroanal. Chem.* **2004**, *564*, 141.

(11) Clavilier, J.; El Achi, K.; Rodes, A. *Chem. Phys.* **1990**, *141*, 1.

(12) Komanicky, V.; Menzel, A.; Chang, K. C.; You, H. *J. Phys. Chem. B* **2005**, *109*, 23543.

(13) *CRC Handbook of Chemistry and Physics*, 85th ed.; Lide, D. R., Ed.; CRC Press: Boca Raton, FL, 2004

(14) Gomez, R.; Climent, V.; Feliu, J. M.; Weaver, M. J. *J. Phys. Chem. B* **2000**, *104*, 597.

(15) Lebedeva N. P., Koper M. T. M., Feliu J. M., van Santen R. A. *J. Phys. Chem. B* **2002**, *106*, 12938.

(16) Panchenko, A.; Koper, M. T. M.; Shubina, T. E.; Mitchell, S. J.; Roduner, E *J. Electrochem. Soc.* **2004**, *151*, 2016.
(17) Gomez, R.; Orts, J. M.; Alvarez-Ruiz, B.; Feliu, J. M. *J. Phys. Chem. B* **2004**, *108*, 228.
(18) Landsberg, R.; Thiele, R. *Electrochim. Acta* **1966**, *11*, 1243.
(19) Ahlberg, E.; Falkenberg, F.; Manzanares, J. A.; Schiffrin, D. J. *J. Electroanal. Chem.* **2003**, *548*, 85.
(20) Rosner, D. E. *J. Electrochem. Soc.* **1966**, *113*, 622.
(21) Schmidt, T. J.; Stamenkovic, V.; Ross, P. N.; Markovic, N. M *Phys. Chem. Chem. Phys.* **2003**, *5*, 400.